Nanoscale

Stabilization of a monolayer tellurene phase at CdTe interfaces

Journal:	*Nanoscale*
Manuscript ID	NR-ART-03-2019-002342.R1
Article Type:	Paper
Date Submitted by the Author:	14-Jun-2019
Complete List of Authors:	Paulauskas, Tadas; University of Illinois at Chicago, Department of Physics Sen, Fatih; Argonne National Laboratory Sun, Ce; University of Texas at Dallas Zhang, Yuan; Argonne National Laboratory Hla, Saw; Argonne National Laboratory Longo, Paolo; Gatan Inc Kim, Moon; the University of Texas at Dallas, Materials Science and Engineering Chan, Maria; Argonne National Laboratory, Center for Nanoscale Materials Klie, Robert; University of Illinois at Chicago, Department of Physics

ARTICLE

Stabilization of a monolayer tellurene phase at CdTe interfaces

Tadas Paulauskas,[a]*† Fatih G. Sen,[b] Ce Sun,[c] Paolo Longo,[d] Yuan Zhang,[b] Saw Wai Hla,[b] Maria K.Y. Chan,[b] Moon J. Kim,[c] and Robert F. Klie[a]

Received 00th January 20xx,
Accepted 00th January 20xx

DOI: 10.1039/x0xx00000x

Two-dimensional (2D) materials provide a plethora of novel condensed matter physics and is the new playground in materials science, offering potentially vast applications. One of the critical hurdles for many 2D systems is the ability to synthesize these low-dimensional systems, as well as to predict and identify new candidates. Herein, a self-assembly of a monolayer tellurene by bonding CdTe wafers is demonstrated for the first time. The conventional applications of wafer-bonding range from production of microelectromechanical systems to synthesis of lattice-mismatched multi-junction photovoltaics. Due to heterogenous materials that are typically employed the bond-interface usually contains a thin amorphous layer or arrays of dislocations. Such interface is thus itself inactive and in many cases produces detrimental effects to the device. The new material phase stabilized in this work consists of an undulating monolayer of tellurium atoms covalently bonded to {111} Cd-terminated CdTe wafer surfaces. First-principles calculations and experimentally observed changes in the localized plasmon excitation energy indicate clear rearrangement of the underlying band-structure suggesting a metallic character, bands showing linear dispersion, and a significant asymmetric spin-band splitting. The I-V characteristics show a presence of a highly conductive pathway that lowers the resistivity by three orders of magnitude, as compared to bulk CdTe, which can be attributed to the tellurium monolayer. The findings indicate that suitably chosen crystallographic wafer surfaces can act as structural templates allowing to produce exotic phases. Presently stabilized monolayer is an addition to the family of tellurene variants, providing new insights into fundamental properties of this and other emerging 2D materials, while bringing attention to the unusual side of the wafer-bonding technology exemplified in this study.

Introduction

Quantum size-effects and dimensional constraints have proven to produce a variety of fascinating materials properties with highly promising applications for future technologies and also stimulating fundamental investigations in the physics offered by these systems. One of the critical hurdles in their study is the ability to synthesize, isolate, and stabilize low-dimensional materials, as illustrated by the case of graphene, the first truly two-dimensional (2D) material. A large group of other 2D materials has been predicted, or already verified, to have exotic properties wildly different from their three-dimensional counterparts. The undulating interfacial Te monolayer stabilized in this work, hereafter referred to as "tellurene", shares some similarities to recently experimentally confirmed 2D tellurene variants.[1] The elemental monolayer and few-layer tellurene in the recent studies were synthesized by several methods, including molecular beam epitaxy, liquid phase exfoliation, as well as substrate-free solution-based methods, demonstrating good stability in air. The resulting tellurene structural arrangements showed dependency on the synthesis method and substrates that were employed, although the most common structure resembles Te bulk-derived trigonal and tetragonal phases.[1-5] Due to the structural complexity, the electronic structure of tellurene variants obtained experimentally and predicted via first-principles calculations also show some spread in its properties. Tellurene is reported with direct as well as indirect bandgaps, ranging between 0.33 to 1.48 eV, carrier mobilities generally higher than MoS_2, and possessing low lattice-thermal conductivity. Applications of tellurene for thermoelectricity are being explored, and two-dimensional tellurene field-effect transistor has been recently demonstrated.[3,5] Lack of inversion symmetry and strong spin-orbit coupling in tellurene encourages applications in spin-transport based devices, among others, while fundamental explorations of this new material system are still ongoing. Tellurium-based structures in general exhibit a variety of properties, including topological semimetals in $MoTe_2$, and topological insulator materials Bi_2Te_3.[6,7] High-pressure phases of the elemental Te range from insulating to superconductive.[8,9] Tellurium atoms in these as well as dichalcogenide structures show a tendency to form planar and helical chain structural units exhibiting low-dimensional transport properties.

Wafer bonding technology, on the other hand, has been utilized for various applications, generally in the fabrication of heterostructures as well as artificial grain boundaries, or bicrystals.[10] For example, arrays of pure edge or mixed screw-edge dislocations with controllable spacing can be produced on-

[a] Department of Physics, University of Illinois at Chicago, Chicago, IL 60607, USA
[b] Center for Nanoscale Materials, Argonne National Laboratory, Lemont, IL 60439, USA
[c] Department of Materials Science and Engineering, the University of Texas at Dallas, Richardson, TX 75080, USA
[d] Gatan Inc., Pleasanton, CA 94588, USA
† Now at Center for Physical Sciences and Technology, Vilnius LT-10257, Lithuania
Electronic Supplementary Information (ESI) available: See OI: 10.1039/x0xx00000x

demand by solid state inter-growing of low-angle miscut crystal wafers.[11] Bicrystals created from $SrTiO_3$ and ZrO_2 wafers, among others, have been employed as substrates for subsequent deposition of superconducting $YBa_2Cu_3O_7$ thin films.[12] Changing the misorientation angle of the bicrystal substrate allows for the critical current of the Josephson junction to be adjusted by several orders of magnitude. Nevertheless, the defect-structures formed at the bond interface in conventional bicrystals typically do not constitute an active layer in the device, and more often than not, introduce detrimental effects.

Here, we report the first synthesis of an interfacial monolayer tellurium phase using ultra-high vacuum bonding of two CdTe wafers. Direct band gap (1.5 eV) zinc blende CdTe, and its related alloys HgCdTe, CdZnTe, are important materials for optoelectronic applications, including radiation detectors, solar cells, infrared imaging.[13] In the course of this study, we fabricated over 20 different CdTe bicrystals and found that only a hand-full of crystallographic surface orientations may allow for the conditions to stabilize a well-defined long-range order exhibiting interfacial structure. In addition to the polar Cd-terminated {111}A CdTe wafers, polar Te-terminated {100}B planes also showed signs of interfacial ordering while preserving Te-rich interfacial chemistry (see Supporting Information S1). These findings suggest that the chemical composition and atomic arrangements of the bonding planes play the role of a structural-template and guides changes in the microscopic degrees of freedom of a bicrystal interface, such as the interfacial atomic relaxations and relative wafer shifts. This suggests that exotic interfacial atomic structures or even chemically heterogeneous interfacial phases could be achieved using this approach, which would otherwise be challenging to stabilize using conventional deposition methods. In the rest of this article, the wafer bonding process and stabilization of the tellurene is described, as well as its experimentally and theoretically obtained structural and electronic properties.

Results

Structural Analysis

The interfacial tellurene was synthesized by the solid state intergrowth (or fusion-bonding) of two single crystal {111}A polar-surface CdTe wafers (more detailed information is provided in *Methods*). The preparation of wafer surfaces included a rinsing in hydrochloric acid. Such chemical polish affects the {111}A surface composition by leaving it Te rich, thus providing necessary Te for the assembly of the monolayer upon bonding. Deposition of Te monolayer on CdTe {111} surfaces by MBE or similar methods could provide an alternative route to prepare the surface chemistry for a such wafer-assisted synthesis.[15] High-angle annular dark-field (HAADF) STEM and atomic-column resolved energy dispersive X-ray spectroscopy (EDS) images of the bicrystal interface region in the <0-11> projection are shown in Figures 1 (a),(b). In this projection, CdTe appears as a collection of closely-spaced atomic-column dumbbells. The interfacial monolayer clearly stands out in STEM images with its distinctive undulating structure. The EDS map in Figure 1 (a) shows Cd-terminated {111}A planes sandwiching the monolayer on either side and also indicates that it is composed solely of tellurium atoms (raw EDS data provided in Supplemental Information, Figure S2). Characterization of the bicrystal samples indicates that uninterrupted patches of the interfacial monolayer tellurene are formed at least up to 20 x 20 *nm* in size. Interfacial atomic facets tend to interrupt the continuous monolayer and transfer it to another parallel {111} plane, as can be seen in Figure 1 (b) and is discussed in more detail below. Improvement of the wafer surfaces and optimization of the bonding process will lead to larger uninterrupted domains of the monolayer.

Based on STEM image analysis, density functional theory (DFT) calculations were used to elucidate a complete tellurene structure (more information provided in *Methods*). The model obtained after DFT structural relaxations of a seed structure is shown in Figure 1 (c)-(e). A perfect match to the experimental structure is obtained reproducing the undulating tellurene as well as more subtle relaxations of the interfacial CdTe atoms. The crystallographic directions drawn in Figure 1 refer to the lower CdTe wafer. The geometry of bonded CdTe wafers can be described here as an incoherent {111}A twin boundary, or more generally as a 180° tilt followed by 180° twist {111}A grain boundary. As a reference to this bonding geometry, an HAADF image of a coherent {111} twin boundary and its Fourier transform are shown in Figure 2 (f),(i), discussed shortly. In the preparation of the seed super-cell structure a rigid-body shift of the wafers with respect to one another was introduced in the amount of half of the repeat distance along the STEM viewing axis <0-11>. This was necessary to obtain the match with experimental images and is in fact required to maintain at least ~2.8 Å inter-atomic Te-Te distances within the tellurene layer. This rigid-body shift also leads to the lack of the crystallographic inversion symmetry with respect to the interfacial plane separating the two CdTe wafers. For a better visualization of the tellurene atomic structure the surrounding CdTe wafer atoms are hidden in Figure 1 (e) and bonds are drawn. Each monolayer atom has four nearest neighbors with inter-atomic distances ranging 3.1 - 3.2 Å and a distorted rhombus shape with bond angles that vary 81°-83° and 95°-98°. The Te-Te interatomic distances in the monolayer and of Te atomic-columns in CdTe bulk are both ~4.7 Å along the STEM imaging <0-11>, thus explaining similar HAADF image contrast of these columns. Examination of the interfacial tellurene structures in Figures 1 (c)-(e) shows that Cd atoms terminating {111} planes near the monolayer are triply bonded on their bulk side of the crystal. Their last tetrahedral bonds naturally extend to the monolayer at nearly right angles to the interface and are fulfilled by the nearest tellurium atoms in tellurene. The bonding chemistry is further examined in the electronic structure section of this manuscript. Modulation of the monolayer can be traced back to tellurene columns being alternatively covalently bonded to the upper and lower hexagonal {111} Cd sheets. The covalent Cd-Te bonds at the interface (2.90 Å *vs.* 2.85 Å bulk CdTe) are bent by ~16° along the <-211> direction, although still at 90° to <0-11>. An in-plane 120°n-rotated view of tellurene (as opposed to Figure 1a and right-hand side of 1 b) is also observed in parts of the bicrystal sample. Our analysis suggests that the change in {111} stacking ordering of planes and the imposed crystallographic symmetry adjacent to tellurene leads to the in-

plane rotation of the monolayer in steps of 120°, creating a sort of a grain boundary between such two domains, as discussed next.

Faceting is the most common type of defect that we observed at the interface. An example of such a defect is seen in Figure 1 (b) and is more clearly shown from another area in the HAADF image of Figure 2 (a). The sequence of CdTe {111} planes (ABCABC…) on each side of the facet is also indicated. A facet on the bonding {111} planes introduces a step to the interface, such that tellurene layer is moved "up" or "down" according to the step height, while still staying between Cd-terminated sheets. The structure on the left-hand-side in Figure 2 (a) is likewise tellurene, although the monolayer is rotated in-plane by 120° around the interface normal giving it a different appearance. This is due to the faceting step, or, more generally, because the encapsulating {111} planes change their sequence (e.g., here C|Te|C to A|Te|B). The stacking sequence induced monolayer rotation can be traced back to the underlying six-fold rotational symmetry of each Cd-sheet to which tellurene is anchored. This type of defect occurs due to the surface roughness of the wafers and is thus strongly dependent on the surface preparation. The HAADF contrast of the Te columns are weaker in the rotated view since the inter-atomic distances are doubled to ~9.4 Å when the monolayer is viewed along the same CdTe <0-11> direction. Accordingly, the distance between the atomic-columns in the image plane is decreased. This is confirmed by quantum mechanical STEM-HAADF image simulations of these separate views from a DFT-relaxed structure in Figures 2 (b)-(c). Figures 2 (d) and (e) show HAADF images of larger area rotated tellurene domains as well as their Fourier transforms (FFT) in Figures 2 (g) and (h), respectively. For a reference, we also included an HAADF image of a common and naturally occurring coherent {111} twin boundary in poly-crystalline CdTe samples in Figure 2 (f), and its FFT in (i). Such a boundary satisfies the full tetrahedral Cd-Te bonding of the interfacial atoms and is electrically inactive. The zone-axes (Z.A.) labeled in Figure 2 (f) is common for all images (d)-(f). The associated indexed and color-coded Bragg spots refer to either the upper (green) or lower (yellow) CdTe crystallites and show an additional 180° twist component in (d) and (e). It is clear that tellurene structure view of Figure 2 (e) introduces image frequencies that appear as a set of vertical lines (arrows) and correspond to a twice larger periodicity in the <-211> direction (horizontal image direction) as compared to the projection of e.g. <1-1-1> Bragg spots onto this direction. The FFT of image (g), however, is seen to be coherent with the bounding CdTe wafers lattice periodicity along <-211> and does not show any essential differences from the FFT of a coherent twin boundary in (i).

Electronic Structure Calculations

Electronic structure calculations at the DFT and many-body perturbation theory levels were performed to elucidate the electronic structure of the interfacial tellurene (details in *Methods*). The total and partial density of states (DOS) of the interfacial system and bulk CdTe, calculated using DFT-PBE, is shown in Figure 3. The total DOS of the tellurene region (black curve) in Figure 3 (a) shows states across the entire bulk CdTe band gap (blue curve). The red DOS curve represents states contributed by only the tellurene monolayer atoms, which was obtained by integrating locally around the interface atoms from the full structure. Analysis of angular momentum-projected DOS (LDOS) indicate that Te atoms in bulk CdTe have solely 5*p*-orbital character at the top of the valence band and a hybrid 5*s*5*p*-character at the bottom of the conduction band.[13] In contrast, the LDOS of tellurene atoms in Figure 2 (b) shows that the states are primarily of *5p* character, with small contributions from the -*s* and -*d* orbitals suggesting a weak -*spd* hybridization. The band-structure of the interface system (i.e., CdTe|tellurene|CdTe) was calculated at special k-points along the *Γ*-*Y*-*S*-*X*-*Γ* direction, i.e., in-plane to tellurene surface, using DFT-PBE with (Figure 3 d) and without (Figure 3 c) of a spin-orbit coupling (SOC). The PBE band-structure shows that tellurene has introduced highly dispersive bands in the bulk CdTe band gap region, with linear dispersions around *S* and *Γ* k-points. The inclusion of SOC in DFT-PBE calculations results in a significant asymmetric splitting of the bands between *Γ*-*Y* (Figure 3d) by 230 meV. The splitting of bands between *Y*-*S* by SOC is also apparent. Band structure of tellurene was also calculated using *GW* without SOC (Supporting Information Figure S3), which shows band crossings between bulk CdTe and tellurene states at the *Y* and *X* k-points, but otherwise similar features to the PBE band structure without SOC. Further splitting of the bands is observed with the inclusion of an electric field of 0.3 eV/Å along the normal direction of the interfacial tellurene plane (Figure 3 e).[16] The amount of charge transfer in the system is calculated using Bader charge analysis, shown in Figure 3 (f).[17,18] The Cd and Te atoms in bulk CdTe have an average charge of +0.5 and -0.5 |e|, respectively, indicating the polar-covalent bonding character. On the other hand, Te atoms in tellurene show very small charge ~-0.1 |e|, similar to what is expected for a metallic system. Electron localization function (ELF) was also used to investigate the chemical bonding nature at the interface.[19] The dimensionless values of ELF range from 0.5 to 1.0, where 0.5 represents a uniform electron-gas system. Higher ELF values can be identified with spatial regions corresponding to covalent bonds and lone-electron pairs. The iso-surfaces of the interface region with ELF=0.85 are plotted in Figure 3 (g). Tetrahedrally coordinated lobes between Cd and Te atoms in bulk CdTe, and analogous regions between the tellurene atoms and nearest Cd neighboring atoms, show polar-covalent bonding. In addition, opposite to the tellurene-bulk Cd atom covalent bonds the large single-lobes on each tellurium atom in tellurene suggest pre-formed lone electron-pairs. Recent studies of tellurene also found similar lone-pairs evidencing their contribution to the metallic-like in-plane bonding and the enhancement of the electronic transport.[20]

Experimental Verifications

Electron energy-loss spectra (EELS) were acquired within a monochromated STEM operated at 60 kV in the same cross-sectional geometry corresponding to Figure 1 (a)-(c). The low-loss region of bulk CdTe exhibits a complex interplay between dispersive volume plasmon excitations and inter-band

transitions originating from Cd-*4d* semi-core states.[21] Three dominant spectral peaks are seen in experimental EELS Figure 4 (d) (red curve, removed zero-loss peak), ~12 eV and ~14 eV are attributed to the inter-band transitions, while the ~16 eV feature is associated to the CdTe volume plasmon and is more pronounced for larger momentum transfers (q). The CdTe volume plasmon in the optical excitation limit (q=0 $Å^{-1}$) is predicted to reside at ~12 eV, according to the Drude model,[21] but appears to compete with single-particle excitations in this energy region. As the beam is scanned towards the interface, a new prominent peak emerges at ~18.3 eV approaching tellurene, while all the bulk CdTe peaks become strongly suppressed (black curve). We note that tellurene low-loss spectrum is inevitably weighted with bulk CdTe features due to the inelastic signal delocalization, which is ~5 *nm* at these excitation energies. The electron energy-loss spectra of bulk CdTe and tellurene system (CdTe|tellurene|CdTe) were calculated from the frequency-dependent dielectric function computed within the G_0W_0 approximation (Supporting Information Figure S4). Tellurene shows a single dominant peak, in general agreement with the measured spectrum in Figure 4 (d). The shift to a lower energy in the calculated tellurene dominant peak position, as compared to the experiment, could arise due to a momentum dependent dispersion of plasmonic excitations that typically show positive relationship with increasing q-transfer. The EEL spectrum was calculated at q=0 $Å^{-1}$, while the experimental q-transfer range continuously from 0 to 0.5 $Å^{-1}$ in the direction transverse to the imaging axis, as defined by the beam convergence angle (see Methods). Based on these considerations we conclude that the observed tellurene low-loss feature represents a damped plasmonic rather than single-particle character of the electronic excitations.

In-plane current-voltage (I-V) measurements were conducted (Figure 4 a-c) to gain further experimental confirmation of the distinct phase formed at the interface. Several different paths (contact placements) were tested (see the inset in Figure 4 a). I-V curves measured on Path 1 (Figure 4 a) are closely linear. The calculated resistivity via a linear fit of the I-V curves (Figure 4 b) at room temperature is ~3E3 ohms·cm, which is 3 orders of magnitude lower than that of bulk CdTe (~1E6 ohms·cm). Despite the fact that the interface becomes less conductive as the temperature drops down, even at 220K the resistivity (~1E5) is still lower than that of bulk CdTe at room temperature. The conductivity was found to be anisotropic for different contact positioning, likely due to interfacial defects. For example, a rectifying behavior for Path 2 is found shown in Figure 4 (c). Although relatively large domains of interfacial tellurene were stabilized in this work, the interface still contains faceting steps and altered tellurene structures due to strain, rotation, etc. It is likely that these defect structures add to the intrinsic resistivity of the interfacial monolayer. The rectification could arise due to the current passing alternatively through the bulk of CdTe as well as domains of the metallic tellurene phases. Nevertheless, the significant increase in the conductivity indicates an additional highly-conductive pathway within the structure which we attribute to the single atomic layer of tellurium formed at the interface. An interface whose atomic tellurium layers are less corrugated will be expected to be more conductive, and its properties more pronounced and accessible to accurate investigations.

Conclusions

The stabilization of the interfacial tellurium phase presented in this study can be attributed to several factors. Firstly, the adjoining close-packed {111}A atomic-planes and the unsatisfied single Cd-covalent bonds act as a structural template for anchoring tellurium atoms. The interface produces atomic-ordering due to atomic-relaxations and spontaneous microscopic wafer-shifts guided by the atomic forces. Chemical treatment of the CdTe wafer surfaces with reagents (here HCl) before bonding plays a key role by influencing the chemical composition of the interface providing Te atoms needed for the monolayer assembly.[22,23] Other routes maybe possible to introduce Te on the surface, such as MBE deposition, or in that matter different species altogether to produce heterogeneous interface layers. Present findings indicate bands showing linear dispersions in the interfacial tellurene and a metallic nature possibly influenced by the pre-formed lone-electron pairs, in addition to a pronounced plasmonic resonance. The large asymmetric spin-band splitting found from the DFT calculations encourages further analysis of such systems for spin-transport based device applications. CdTe is known to be amenable to *n*- as well as *p*- doping, which can provide additional means to tune the chemical potential at the interface by bonding doped wafers. A further inquiry into such synthesis would be experimental and computational studies of bonding close-packed polar surfaces in other II-VI, III-V zinc-blende and wurtzite materials or their alloys. The interfacial tellurene created hereby via wafer bonding marks the first system to be stabilized in this manner. These findings suggest that wafer bonding could provide an access to exotic and non-stoichiometric phases unique to this synthesis approach, constituting a new tool in the engineering of materials.

Methods

Fabrication of tellurene

Tellurene was fabricated by bonding two single crystal CdTe wafers with face-to-face oriented Cd-terminated {111} crystal planes. High-purity undoped, 10 × 10 mm^2 CdTe {111} wafers with a thickness of 3 *mm* were used for the bonding experiments. Out-of-plane ($2\vartheta/\omega$ scan) and in-plane (φ scan) X-ray diffraction (XRD) (Ultima III, Rigaku) was used to determine the crystal orientations of the planes and flats. The root-mean-square (RMS) surface roughness was measured to be less than 1 *nm* by atomic-force microscopy (AFM) (Dimension 3100, Veeco) in a tapping mode. Samples were rinsed in de-ionized water for 5 s, dipped in hydrochloric acid (15% HCl) for 30 s, and rinsed again in de-ionized water for 5 s. The samples were subsequently dried under a flow of nitrogen gas and heated on a hot-plate at 110 °C for 5 s to evaporate de-ionized water. The wafer-pairs were then loaded into a vacuum bonder (EV 501), maintaining 400°C temperature for 20 hrs under a pressure of 1

MPa. Tellurene was also successfully recreated with this same fabrication method using another pair of CdTe wafers.

STEM imaging, XEDS and EELS

Cross-sectional STEM samples of the interface for STEM/XEDS imaging and EELS acquisition were prepared using a focused electron/ion-beam (FIB, FEI Nova 200). The samples were thinned and polished to less than 30 nm thickness, and Ar plasma-cleaned before loading into a STEM instrument. Atomic-resolution Z-contrast images and XEDS mappings were collected with a probe spherical aberration-corrected cold-field emission JEOL JEM ARM-200CF scanning-transmission electron microscope located at the University of Illinois at Chicago. It is operated at 200 keV beam energy; the beam convergence semi-angle was set to 28 mrad resulting in a probe size of approximately 80 *pm* and a probe current of 19 pA. A windowless XEDS silicon drift-detector X-Max^N 100TLE from Oxford Instruments was used to collect atomic-column resolved X-ray spectrum images. To obtain sufficient X-ray signal, the probe size was increased to 130 pm, providing approximately 140 pA of probe current at the same convergence angle. STEM electron energy-loss spectra (EELS) was acquired at the Ohio State University using 60 keV beam energy, 10 mrad probe convergence semi-angle, 50 mrad collection angle, 0.025 eV energy dispersion, and 0.15 eV energy resolution. No noticeable damage, alterations or material loss of the interfacial monolayer was observed during STEM data acquisitions. This provides support that the tellurene is formed during the wafer-bonding process rather than as a result of the electron beam irradiation. STEM HAADF image simulations on the atomically relaxed DFT structures were performed using *μSTEM* multislice software (tcmp.ph.unimelb.edu.au/mustem) with the experimental STEM parameters and 20 *nm* sample thickness. The simulations included thermal diffuse-scattering effects within the frozen-phonon approximation.

First-principles calculations

The electronic structure of tellurene is analyzed using density functional theory (DFT) and many body perturbative *GW* calculations. All DFT and *GW* calculations were carried out using the plane-wave-based Vienna Ab initio Simulation Package (VASP).[24,25] Projector augmented wave (PAW) potentials were used, and the exchange-correlation was treated with the generalized gradient approximation (GGA) parameterized by Perdew, Burke, and Ernzerhof (PBE).[26,27] Accurate band structure is obtained using the *GW* approximation in the form of one-shot *GW* (G_0W_0), with quasiparticle energies from Wannier interpolation via the WANNIER90 program.[28-33] Wannier functions are projected using Cd *s* and *d*, and Te *s* and *p* orbitals. PBE calculations were carried out at the Γ-centered 10×6×1 k-point grid, whereas *GW* calculations used 4×2×1 k-point grid in the Brillouin zone. The plane-wave kinetic energy cutoff was 274.3 eV. Atomic positions were relaxed until forces are below 0.05 eV/Å and electronic relaxation was converged to 10^{-5} eV to ensure convergence to 1-2 meV/atom in total energy. The electronic charges on atoms in DFT calculations are obtained by partitioning the charge density according to atomic positions in the crystal based on the Bader charge analysis, as implemented in VTST-scripts.[17,18] Tellurene atomic structure is constructed according to the STEM images as stacked between 3 CdTe {111} planes on both sides, with the stacking represented by *ABC*|Te|*CBA*. The interface slab had a 15 Å vacuum in the z-direction to prevent interactions between periodic images and Te atoms on the surface are terminated with H atoms with 0.5 $|e|$.

I-V measurements

The contacts were formed at the bond interface at four points around the bond perimeter, as shown in Figure 3a, using a conductive 2-component epoxy silver glue, covering approximately 1.5 mm area. Bonding gold wires were soldered to a measurement stand and resistances of each contact were accounted for in the experiment. I-V curves were collected at different temperatures. Since the sample became insulating below ~160K, the data was collected from 170K to 300K.

Conflicts of interest

There are no conflicts to declare.

Acknowledgements

This work was supported in parts by the U.S. Department of Energy through the EERE-Sunshot BRIDGE (DE-EE0005956) and PVRD (DE-EE 0007545) programs. The authors acknowledge John Mitchell and Olle Heinonen for helpful discussions. The authors thank D.W. McComb and R.E.A. Williams at the Center for Electron Microscopy and Analysis (cemas.osu.edu) at The Ohio State University for granting access to the monochromated FEI Titan as well as assistance with aligning the monochromator. This work was also partially supported by the Louis Beecherl, Jr. endowment funds, the Center for Low Energy Systems Technology (LEAST), one of the six SRC STARnet Centers, sponsored by MARCO and DARPA, and the SWAN Center, a SRC center sponsored by the Nanoelectronics Research Initiative and NIST. Use of the Center for Nanoscale Materials, an Office of Science user facility, was supported by the U. S. Department of Energy, Office of Science, Office of Basic Energy Sciences, under Contract No. DE-AC02-06CH11357. This research used resources of the National Energy Research Scientific Computing Center, a DOE Office of Science User Facility supported by the Office of Science of the U.S. Department of Energy under Contract No. DE-AC02-05CH11231. This work used the Extreme Science and Engineering Discovery Environment (XSEDE), which is supported by National Science Foundation grant number ACI-1053575. MJK was supported in part by Global Research and Development Center Program (2018K1A4A3A01064272) and Brain Pool Program (2019H1D3A2A01061938) through the National Research Foundation of Korea (NRF) funded by the Ministry of Science and ICT.

References

1 Wenzhuo Wu, Gang Qiu,Yixiu Wang, Ruoxing Wang and Peide Ye, Chem. Soc. Rev., (2018), 47, 7203-7212.
2 Zhili Zhu, Xiaolin Cai, Seho Yi, Jinglei Chen, Yawei Dai, Chunyao Niu, Zhengxiao Guo, Maohai Xie, Feng Liu, Jun-Hyung Cho, Yu Jia, and Zhenyu Zhang, PRL 119, 106101 (2017).
3 Sitansh Sharma, Nirpendra Singh, and Udo Schwingenschlögl, ACS Appl. Energy Mater. 2018, 1, 1950−1954.
4 Jiahuan Yan, Xiuying Zhang, Yuanyuan Pan,a Jingzhen Li, Bowen Shi, Shiqi Liu, Jie Yang, Zhigang Song, Han Zhang, Meng Ye, Ruge Quhe, Yangyang Wang, Jinbo Yang, Feng Pan, and Jing Lu, J. Mater. Chem. C 6, 6153-6163, (2018).
5 Yixiu Wang, Gang Qiu, Ruoxing Wang, Shouyuan Huang, Qingxiao Wang, Yuanyue Liu, Yuchen Du, William A. Goddard III, Moon J. Kim, Xianfan Xu, Peide D. Ye & Wenzhuo Wu, Nature 1, 228–236 (2018).
6 Qi, Y.; Naumov, P. G.; Ali, M. N. Rajamathi, C. R. Schnelle, W. Barkalov, O. Hanfland, M.; Wu, S.C., Shekhar, C. Sun, Y., Nature Communications 2016, 7, 11038.
7 Huang L. McCormick, T. M. Ochi, M. Zhao Z., Suzuki, M.T. Arita, R., Wu, Y., Mou D., Cao, H., Yan, J., Nature Materials 2016, 15, 1155-1160.
8 Sheldrick, W. S., Wachhold, M., Jobic, S., Brec, R. & Canadell, E. Advanced Materials 9, 669-675, (1997).
9 Wang, Q., Safdar, M., Wang, Z. & He, J. Advanced Materials 25, 3915-3921, (2013).
10 H Moriceau, F Rieutord, F Fournel, Y Le Tiec, L Di Cioccio, C Morales, A M Charvet and C Deguet, Adv. Nat. Sci.: Nanosci. Nanotechnol. 1 (2010) 043004.
11 Ce Sun, Tadas Paulauskas, Fatih G. Sen, Guoda Lian, Jinguo Wang, Christopher Buurma, Maria K. Y. Chan, Robert F. Klie and Moon J. Kim, Scientific Reports volume 6, 27009 (2016).
12 P. A. Nilsson, Z. G. Ivanov, H. K. Olsson, D. Winkler, T. Claeson, E. A. Stepantsov and A. Zalenchuk, Journal of Applied Physics 75, 7972 (1994).
13 Triboulet, R. & Siffert, P. CdTe and Related Compounds; Physics, Defects, Hetero-and Nano-structures, Crystal Growth, Surfaces and Applications: Physics, CdTe-based Nanostructures, CdTe-based Semimagnetic Semiconductors, Defects. (Elsevier, 2009).
14 P. Norton, Opto-Electronics Review 10(3), 159–174 (2002)
15 Wu, T., Chen, J., Chiang, C., Pang, Y. & Yang, S. Journal of applied physics 71, 5212-5216 (1992).
16 Yuan, H. et al. Nature Physics 9, 563-569 (2013).
17 Bader, R. F. Atoms in molecules. (Wiley Online Library, 1990).
18 Henkelman, G., Arnaldsson, A. & Jonsson, H. Comp. Mater. Sci. 36, 354-360 (2006).
19 Becke, A. D. & Edgecombe, K. E. The Journal of chemical physics 92, 5397-5403 (1990).
20 Yuanyue Liu, Wenzhuo Wu, and William A. Goddard, J. Am. Chem. Soc., 2018, 140 (2), pp 550–553
21 Dröge, H. et al. Physical Review B 59, 5544 (1999).
22 Ivanits'ka, V. et al. Journal of Electronic Materials 36, 1021-1024 (2007).
23 Lu, Y. C., Stahle, C., Feigelson, R. & Morimoto, J. Journal of applied physics 62, 4453-4459 (1987).
24 Kresse, G. & Furthmuller, J. Computational Materials Science 6, 15-50, (1996).
25 Kresse, G. & Furthmuller, J. Physical Review B 54, 11169-11186, doi:10.1103/PhysRevB.54.11169 (1996).
26 Kresse, G. & Joubert, D. Physical Review B 59, 1758-1775, doi:10.1103/PhysRevB.59.1758 (1999).
27 Perdew, J. P., Burke, K. & Ernzerhof, M. Physical Review Letters 77, 3865-3868, doi:10.1103/PhysRevLett.77.3865 (1996).
28 Hedin, L. Physical Review 139, A796 (1965).
29 Fuchs, F., Furthmüller, J., Bechstedt, F., Shishkin, M. & Kresse, G. Physical Review B 76, 115109 (2007).
30 Shishkin, M. & Kresse, G. Physical Review B 74, 035101 (2006).
31 Marzari, N. & Vanderbilt, D. Physical review B 56, 12847 (1997).
32 Mostofi, A. A. et al. Computer physics communications 178, 685-699 (2008).
33 Souza, I., Marzari, N. & Vanderbilt, D. Physical Review B 65, 035109 (2001).

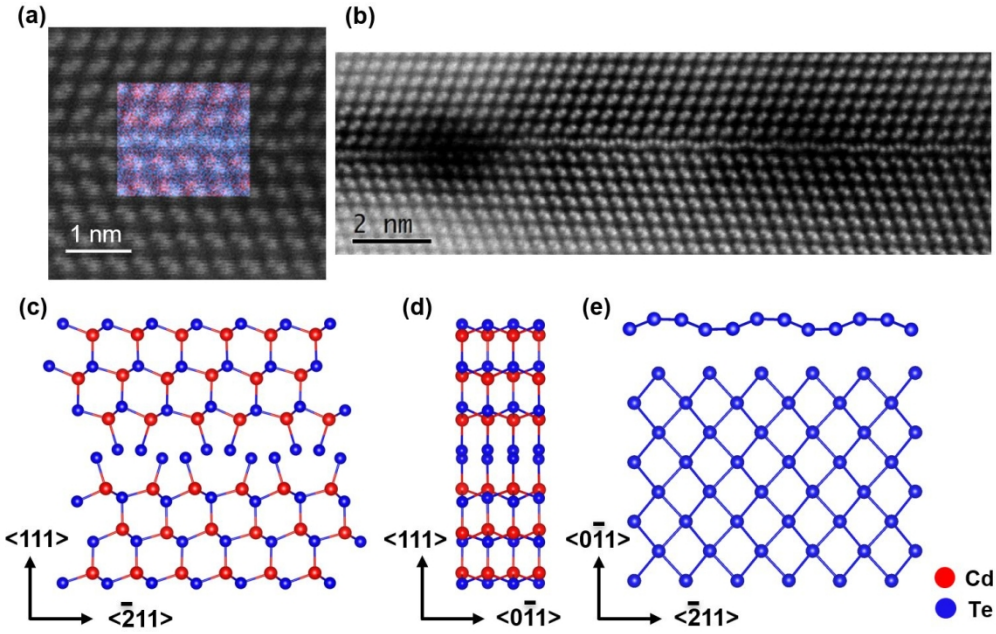

Figure 1. (a) Atomic-resolution X-ray spectrum image (Lα1 emissions, Cd-red, Te-blue) of the interface overlaid on the Z-contrast HAADF image. (b) Lower magnification HAADF image of the interface showing a larger section of tellurene. A defect structure is seen on the left side. HAADF images were taken along CdTe <0-11>. (c)-(e) Structure obtained by DFT relaxation based on STEM images. (c) the model along CdTe <0-11>, suggested covalent bonds are represented by lines. (d) 90° rotated structure around the interface normal. (e) Top view of the tellurene layer, CdTe wafers atoms are hidden and bonds are drawn for better visualization. Crystallographic directions refer to the lower CdTe wafer.

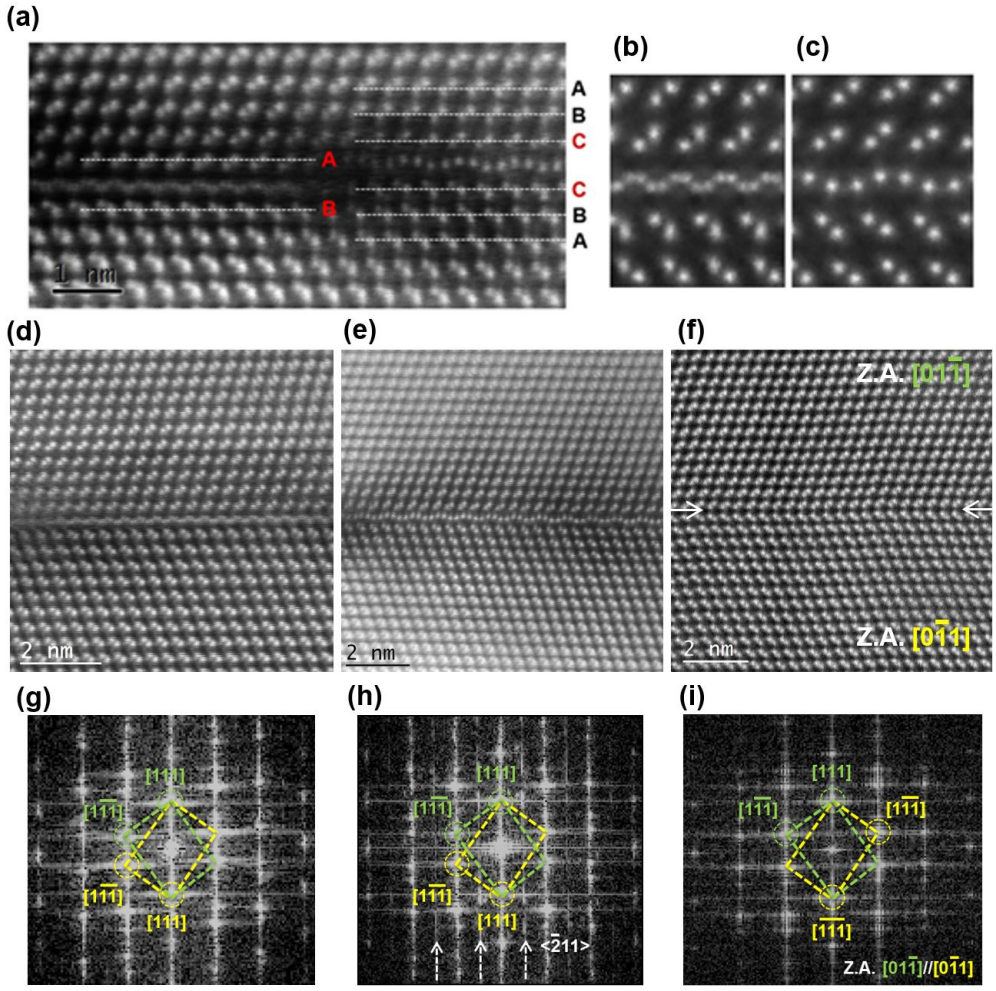

Figure 2. (a) HAADF image of a faceting defect-induced relocation of the tellurene by one atomic plane and the associated in-plane rotation of the monolayer. Stacking sequence of {111} planes are indicated. (b) Simulated HAADF image of the 120° rotated tellurene corresponding to the left-hand side of Figure 2 (a). (c) Simulated HAADF of the right-hand side Fig. 2 (a). (d), (e) HAADF images of larger areas of the different tellurene views, and their Fourier transforms, (g) and (h), respectively. (f) Image of a coherent twin boundary in poly-crystalline CdTe, for a reference, and its Fourier transform in (i). Zone-axes are indicated for the upper and lower CdTe wafers, and are common for all the HAADF images in Figure 2.

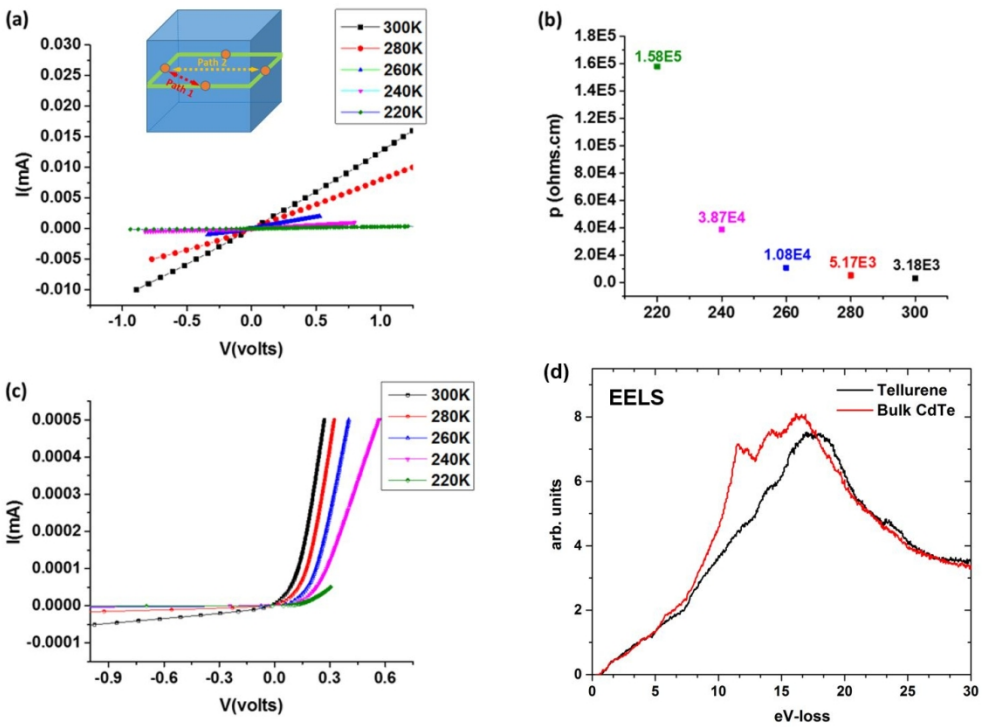

Figure 4. (a)-(c) Current-voltage (I-V) characteristics of the tellurene bicrystal structure at various temperatures. (a) I-V measurements corresponding to contacts placed for Path 1 in the inset. Green lines mark perimeter of the interface. (b) Linear fit of curves in (a) showing the resistivity versus temperature. (c) I-V curve for Path 2 suggesting a rectifying behavior, likely due to corrugated interface. (d) Electron energy-loss spectra of bulk CdTe and tellurene interface acquired in STEM.

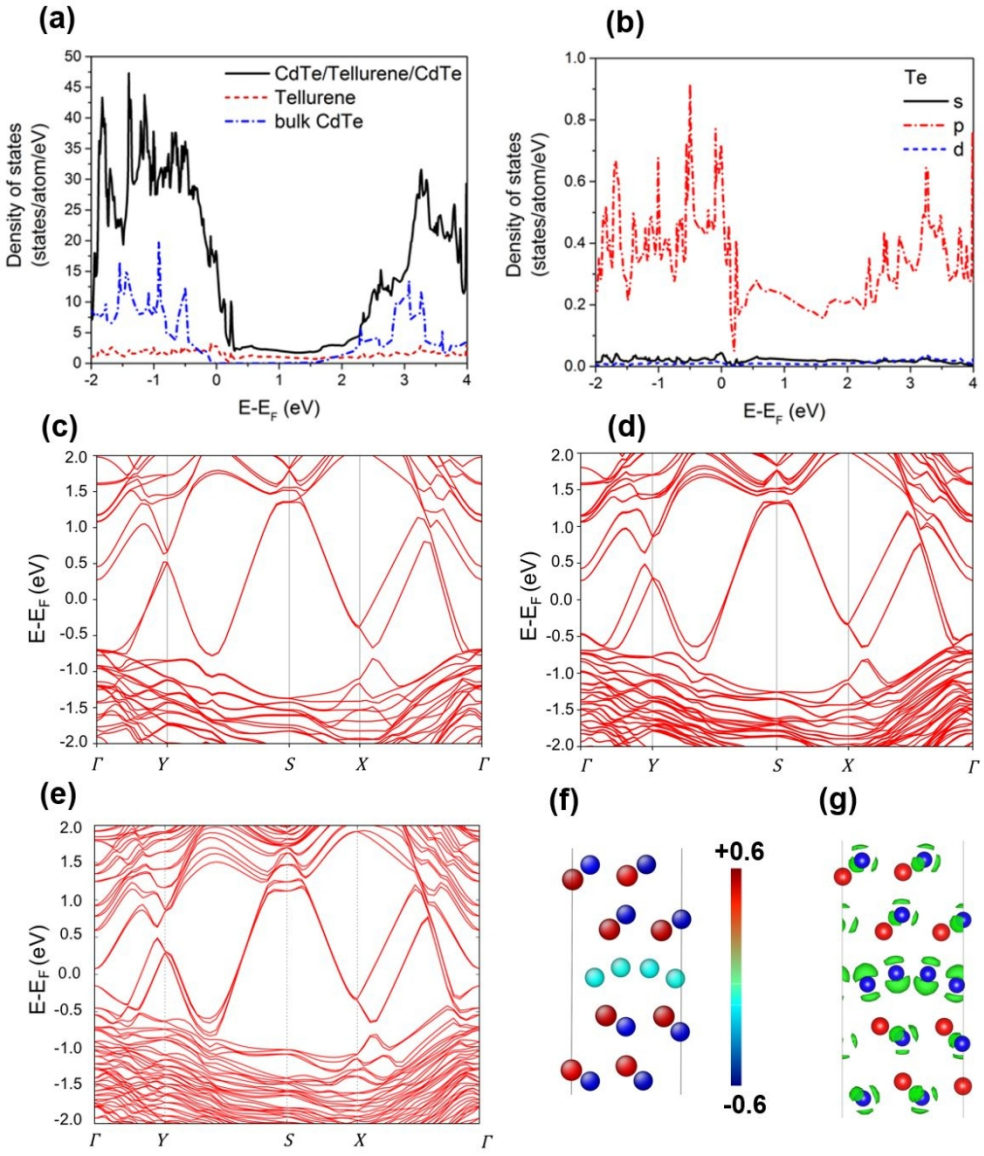

Figure 3. Electronic structure calculated from DFT-PBE: (a) total density of states (DOS) of tellurene system compared with bulk CdTe, and locally integrated DOS of tellurene monolayer. (b) Angular momentum-decomposed density of states (LDOS) of the Te atoms in tellurene structure. (c) In-plane band structure of tellurene system, without (c) and with (d) spin-orbit coupling (SOC). Large asymmetric spin-band splitting can be seen near Y point. (e) Band structure with SOC and external electric-field perpendicular to the interface plane. (f) Bader charge of interface atoms, (g) electron localization function (ELF) iso-surfaces (green) with ELF=0.85 are shown.

Monolayer tellurene phase created between two CdTe crystals via wafer bonding.